A GAN-GRU Based Space-Time Predictive Channel Model for 6G Wireless Communications

Zheao Li, Cheng-Xiang Wang, *Fellow, IEEE*, Chen Huang, *Member, IEEE*, Jie Huang, *Member, IEEE*, Junling Li, *Member, IEEE*, Wenqi Zhou, and Yunfei Chen, *Senior Member, IEEE*

***Abstract*—The advent of sixth-generation (6G) wireless communications has posed significant challenges to channel modeling. Channel measurements cannot cover all scenarios and frequency bands for 6G, and conventional models lack accurate predictive capabilities. To address these issues, this paper proposes a novel 6G space-time joint predictive channel model to predict channels in the space-time domains, which can rebuild lost measurement data and correct abnormal data. The proposed model designs a space-time generative adversarial network (STGAN) framework, conditioned on channel large-scale and small-scale characteristics, to synthesize sufficient space-time channel datasets, effectively overcoming data shortages. Accompanied by path identification and characteristic classification, the coupled gated recurrent unit (GRU) framework conducts precise predictions for unknown channels in the space-time domains. Comprehensive experiments demonstrate the proposed model's superiority over other methods, including the geometry-based stochastic channel model (GBSM), GRU, long short-term memory (LSTM), and radial basis function neural network (RBF-NN). The model's effectiveness can be attributed to its architecture to capture complex space-time variations and accurately predict non-linear channel characteristics based on continuous measurements. Validation on both indoor and outdoor channel measurements further confirms the model's generality and accuracy. The proposed model provides a robust solution in the space-time joint channel prediction for advanced wireless communications.**

***Index Terms*—6G wireless communications, channel space-time joint characteristics, generative adversarial network, machine learning, predictive channel modeling.**

This work was supported by the National Natural Science Foundation of China (NSFC) under Grants 61960206006, 62271147, 62301364, and 62301151, the Key Technologies R&D Program of Jiangsu (Prospective and Key Technologies for Industry) under Grants BE2022067, BE2022067-1, and BE2022067-3, the Fundamental Research Funds for the Central Universities under Grant 2242022k60006 and 2242023K5003, the EU H2020 RISE TESTBED2 project under Grant 872172, the High Level Innovation and Entrepreneurial Doctor Introduction Program in Jiangsu under Grant JSSCBS20210082, the Fellowship of China Postdoctoral Science Foundation under Grants 2021M702499, the Outstanding Postdoctoral Fellow Program in Jiangsu, Young Elite Scientists Sponsorship Program by CAST under Grant 2022QNRC001, and the Start-up Research Fund of Southeast University under Grant RF1028623029. (*Corresponding Authors: Cheng-Xiang Wang and Chen Huang.*)

Z. Li, C.-X. Wang, J. Huang, J. Li, and W. Zhou are with the National Mobile Communications Research Laboratory, School of Information Science and Engineering, Southeast University, Nanjing 210096, China, and also with the Purple Mountain Laboratories, Nanjing 211111, China (email: {li_zheao, chxwang, j_huang, junlingli, wqzhou}@seu.edu.cn).

C. Huang is with the Purple Mountain Laboratories, Nanjing 211111, China, and also with the National Mobile Communications Research Laboratory, School of Information Science and Engineering, Southeast University, Nanjing 210096, China (email: huangchen@pmlabs.com.cn).

Y. Chen is with the Department of Engineering, University of Durham, Durham, U.K. OHI 3LE (email: Yunfei.Chen@durham.ac.uk).

I. Introduction

The remarkable development and widespread applications of the sixth generation (6G) wireless communications have put forward very high requirements on the accuracy of network-level performance [1], [2]. Evolving from the fifth generation (5G) wireless communications, 6G plans to continue to enhance the mobile Internet and Internet of Everything (IoE), and also deeply integrate them with artificial intelligence (AI) and big data to realize the intelligent IoE. The 6G vision can be summarized as global coverage, all spectra, full applications, all senses, all digital, and strong security [3], [4]. Global coverage means that 6G plans to expand the current terrestrial wireless communication systems to the space-air-ground-sea integrated communication systems. To meet the massive traffic and connectivity requirements in all spectra, 6G frequency bands will include the sub-6 GHz, millimeter wave (mmWave), terahertz, and optical wireless bands. New technologies, such as AI and big data, can be fully utilized to explore the intelligent potential of 6G communications and realize full applications. The vision of all senses means all five human senses can be transmitted through 6G communications to achieve the fusion of virtuality and reality. Through the interconnection of the real physical world and the virtual digital world, 6G plans to realize the all digital vision. Strong security is to construct secure communications, including physical layer and network layer security, to achieve endogenous security.

As an important part of 6G communications, wireless channels are the medium of information exchange, whose characteristics are determined by the propagation environment. Traditional channel research often follows four steps, i.e., channel measurement, channel parameter estimation, channel characteristic analysis, and channel modeling. They are the foundations of system design, theoretical analysis, performance evaluation, and optimization of wireless communications [5]. Channel modeling is used to analyze the influence of different wireless channels on the transmitted signals. It provides effective and feasible simulations of different radio wave propagation scenarios [3]. By introducing new frequency bands, new techniques, and new scenarios, 6G wireless channels present new characteristics that need to be explored through channel measurements and channel characterization. However, for 6G, a number of new problems and challenges occur using conventional channel modeling methods. The complicated and diverse communication scenarios entail high-performance channel sounders at extremely high cost and manpower. It is impossible to conduct channel measurements for

all frequency bands in all scenarios. Besides, processing a large amount of channel measurement data requires high-resolution parameter estimation methods, which incur extremely high complexity. It is also not possible to fully explore the complicated relationship between new characteristics, frequencies, and scenarios using conventional mathematic channel models. Finally, conventional channel models can only provide limited channel characterization and are unable to predict channel characteristics in the future time, unknown frequency bands, and unknown scenarios. Due to the above problems, novel channel modeling methods for 6G are motivated.

With the dramatic development of AI in the last few decades, the deep integration of AI and communications will be one of several key technologies for the construction and development of future communications [6]–[8]. As an essential branch of AI, machine learning (ML) has a good ability to learn and extract potential features that conventional modeling methods cannot obtain [9]. Besides, it can also effectively and accurately estimate parameters and predict channel characteristics for many scenarios. Due to the unique characteristics of non-linear function expression and feature extraction, the combination of ML and channel modeling has accelerated the in-depth research on sophisticated technologies [10]–[15]. In [16], an ML-based channel model was presented to predict the angle of arrival (AoA) based on real vehicular measurement datasets by the support vector machine (SVM). An artificial neural network (ANN) based channel modeling and simulation framework was used in [17] to predict the received power, delay spread (DS), angle spread (AS), and cross-polarization ratio at each location to playback multiple-input multiple-output (MIMO) channels. In [18], the paper introduced the ML algorithm into the path loss (PL) model to capture the structure-related characteristics when modeling channels in the near-ground segment. An ML-based channel parameter prediction method was proposed in [19] by using the feed-forward neural network (FNN) and radial basis function neural network (RBF-NN). By learning the channel characteristics of the mmWave massive MIMO channel, such as the received power, DS, and AS, the model achieved good performance in channel parameter prediction. The authors in [20] introduced a long short-term memory (LSTM)-based satellite communication channel prediction method to estimate the received power, and obtained good performance in the sequence-related data prediction. In [21], a novel receiver architecture using the recurrent neural network (RNN) was proposed by learning the channel variations to predict channel fade coefficients in time-variant channels. A deep transfer learning-based downlink channel prediction method was presented in [22] with the meta-learning algorithm, where the network was trained in the manner of the fully-connected neural network and was then fine-tuned for the new environment. A CsiPreNet was proposed [23] by integrating the convolutional neural network (CNN) and LSTM to predict an underwater acoustic channel in the frequency domain.

On the one hand, while existing ML-based channel modeling approaches have achieved success, they often fail to integrate channel characteristics in their prediction framework. It lacks a comprehensive analysis of network structures and features about channel characteristics, particularly channel large-scale and small-scale fading. Furthermore, previous channel parameters prediction based on discrete datasets [16], [17], [19], [24], [25] are not able to be applied to continuous channel modeling and characterization directly with unknown information, leading to limited applicability in specific domains.

On the other hand, traditional space-domain and time-domain channels are modeled separately [13], requiring a large number of channel measurement data at different locations and times to capture corresponding characteristics. However, continuous movement changes of users in spatial locations and environments also cause channel variations in the time domain, so channel space-time characteristics are often coupled simultaneously and jointly. The difficulty of constructing the space-time joint predictive channel model lies in capturing the continuous channel variations at each location in the time series. Due to the time-consuming and expensive channel measurement campaigns, it is hard to collect enough high-precision channel data with sufficient space-time characteristics, so there is a great reliance on the amount of training data when using ML to do the space-time channel prediction. Compared with other ML methods, generative adversarial network (GAN) [26] can generate clearer and more realistic samples with lower complexity, and can effectively solve the insufficient dataset issue in 6G. There are several studies on channel modeling using GAN. In [27], a novel GAN framework was proposed to solve the problem of autonomous wireless channel modeling without complex theoretical analysis or data processing. A novel GAN-based channel model is proposed in [28] to model single-input single-output (SISO) channel time-frequency response, which considers the time-frequency response of the channel as an image. However, the authors only considered the feasibility of channel modeling by GAN with simple experiments. The authors in [29] and [30] proposed a ChannelGAN and some novel GAN-based channel simulation architectures to accurately synthesize channel data with good performance. A trained GAN was used in [31] to produce the random angle offsets in the proposed ML-based 3-D channel model to generate random parameters for channel modeling. In [32], a GAN-based channel modeling method was proposed for a digital twin (DT) channel, which can generate identical statistical distribution with measured channels. While these ML-based channel modeling efforts have shown promise, they exhibit certain limitations on conducting the space-time joint channel prediction from the known channel characteristics based on insufficient channel data.

To the best of the authors' knowledge, there is currently a lack of research on acquiring sufficient channel datasets and developing the space-time joint channel prediction methods for 6G communications. To fill the research gaps, a novel GAN and gated recurrent unit (GRU) based joint predictive channel model is proposed in this paper. The main contributions and novelties of this paper are summarized as follows.

- A novel space-time joint predictive channel modeling methodology is exploited to effectively capture continuous channel variations at each location in a time series. By utilizing a group of channel evolutional patterns, the GAN-GRU based predictive channel model can rebuild

lost data and correct abnormal data to improve prediction accuracy, thereby demonstrating the importance of the space-time joint channel prediction. Compared to existing methods, the GAN-GRU framework is among the first to perform the space-time joint channel prediction and has better accuracy and efficiency in generating parameters.

- A space-time GAN (STGAN) framework is designed in the proposed predictive channel model to solve the problem of insufficient dataset acquisition. Conditioned on channel large-scale and small-scale characteristics, the STGAN-based framework is good at synthesizing channel datasets with the space-time characteristics and expands the channel dataset based on real measurement data. When considering the similarity and diversity of synthetic data, this approach shows good performance of data augmentation in comparisons, which is particularly useful for improving the training performance of the space-time joint channel prediction.
- A coupled GRU framework is designed in the proposed predictive channel model to jointly predict unknown channels in the space-time domains. By identifying the path with the strongest power in the line-of-sight (LoS) and non-LoS (NLoS) scenarios to classify channel large-scale fading and small-scale fading, the proposed model can separately extract and learn the space-time joint characteristics. Besides, it can use previous channel data obtained by continuous measurements to predict the next channel in the space-time domains.
- Prediction experiments are conducted by using our measurement data performed in an indoor corridor. The proposed model is evaluated and compared to the traditional geometry-based stochastic channel model (GBSM) and several widely used ML-based predictive channel modeling methods, including normal GRU, LSTM, and RBF-NN. The proposed model achieves better prediction performance than these methods, in terms of root mean square error (RMSE) and mean absolute percentage error (MAPE). The prediction performance criteria between the channel measurement data and prediction data are less than 6 dB and 6%, respectively. Moreover, the generality of the proposed model is validated on an outdoor channel measurement dataset.

The remainder of this paper is organized as follows. Section II summarizes the problem description of the space-time joint channel prediction. The GAN-GRU based joint space-time predictive channel model is presented in Section III. Section IV explains the channel measurement and algorithm implementation. In Section V, experimental results and analysis are provided and compared with those of other methods. Finally, conclusions are drawn in Section VI.

II. Problem Description

Wireless channels are represented by the channel impulse response (CIR) matrix $\mathbf{H_s} = [h_{qp,f_c}(t,\tau)]_{M_R \times M_T}$, where the elements $h_{qp,f_c}(t,\tau)$ of the matrix represent the CIR between the pth transmitter (Tx) and qth receiver (Rx) antenna elements, f_c is the carrier frequency, M_R is the number of Rx, and M_T is the number of Tx. The 6G pervasive channel model (6GPCM) [33] is a kind of GBSM that uses a unified CIR to integrate typical channel characteristics at different frequency bands and scenarios for 6G. Using the 6GPCM, the traditional mathematic CIR can be expressed as

$$h_{qp,f_c}(t,\tau) = \sqrt{\frac{K_R(t)}{K_R(t)+1}} h^L_{qp,f_c}(t,\tau) + \sqrt{\frac{1}{K_R(t)+1}} h^N_{qp,f_c}(t,\tau) \tag{1}$$

where $K_R(t)$ is the Rician K-factor at time t, $h^L_{qp,f_c}(t,\tau)$ is the LoS component, and $h^N_{qp,f_c}(t,\tau)$ is the NLoS component.

$$h^L_{qp,f_c}(t,\tau) = \begin{bmatrix} F_{q,f_c,V}(\phi^R_{E,L}(t),\phi^R_{A,L}(t)) \\ F_{q,f_c,H}(\phi^R_{E,L}(t),\phi^R_{A,L}(t)) \end{bmatrix}^T \begin{bmatrix} e^{j\theta^{VV}_L} & 0 \\ 0 & -e^{j\theta^{HH}_L} \end{bmatrix} \mathbf{F_r} \begin{bmatrix} F_{p,f_c,V}(\phi^T_{E,L}(t),\phi^T_{A,L}(t)) \\ F_{p,f_c,H}(\phi^T_{E,L}(t),\phi^T_{A,L}(t)) \end{bmatrix} e^{j2\pi f_c \tau^L_{qp}(t)} \delta(\tau - \tau^L_{qp}(t)) \tag{2}$$

$$h^N_{qp,f_c}(t,\tau) = \sum_{n=1}^{N_{qp}(t)} \sum_{m=1}^{M_n(t)} \begin{bmatrix} F_{q,f_c,V}(\phi^R_{E,m_n}(t),\phi^R_{A,m_n}(t)) \\ F_{q,f_c,H}(\phi^R_{E,m_n}(t),\phi^R_{A,m_n}(t)) \end{bmatrix}^T \begin{bmatrix} e^{j\theta^{VV}_{m_n}} & \sqrt{\mu k^{-1}_{m_n}(t)} e^{j\theta^{VH}_{m_n}} \\ \sqrt{k^{-1}_{m_n}(t)} e^{j\theta^{HV}_{m_n}} & \sqrt{\mu} e^{j\theta^{HH}_{m_n}} \end{bmatrix} \mathbf{F_r} \begin{bmatrix} F_{p,f_c,V}(\phi^T_{E,m_n}(t),\phi^T_{A,m_n}(t)) \\ F_{p,f_c,H}(\phi^T_{E,m_n}(t),\phi^T_{A,m_n}(t)) \end{bmatrix} \sqrt{P_{qp,m_n,f_c}(t)} e^{j2\pi f_c \tau_{qp,m_n}(t)} \delta(\tau - \tau_{qp,m_n}(t)) \tag{3}$$

where $\{\cdot\}^T$ represents transposition operation, and $F_{p,f_c,V}$, $F_{q,f_c,V}$, $F_{p,f_c,H}$, and $F_{q,f_c,H}$ are the antenna patterns of A^T_p or A^R_q for vertical and horizontal polarizations at f_c, respectively. ϕ^T_A, ϕ^T_E, ϕ^R_A, and ϕ^R_E are azimuth angle of departure, elevation angle of departure, azimuth angle of arrival, and elevation angle of arrival, respectively. Note that in this paper, $N_{qp}(t)$ is the number of clusters, $M_n(t)$ is the number of sub-rays in the cluster, $k_{m_n}(t)$ is the cross-polarization power ratio, $\mathbf{F_r}$ is the rotation matrix, μ is the co-polar imbalance. θ^{VV}_L, θ^{HH}_L, $\theta^{VV}_{m_n}$, $\theta^{VH}_{m_n}$, $\theta^{HV}_{m_n}$, and $\theta^{HH}_{m_n}$ are the initial phases with uniform distribution over $(0, 2\pi]$. $P_{qp,m_n,f_c}(t)$ and $\tau_{qp,m_n}(t)$ are the power and delay from pth antenna to qth antenna of the mth ray in the nth cluster, respectively.

By introducing new frequency bands, new techniques, and new scenarios, 6G wireless channels present new characteristics that need to be explored through channel prediction in different domains. Thus, we construct an ML-based predictive channel modeling architecture, as demonstrated in Fig. 1. This architecture covers the space-time-frequency predictive channel modeling systems in one framework to include different characteristics in these domains. According to (1), the predictive channel modeling mechanisms in these three domains are similar: constructing a predictive model that can learn the channel evolution patterns in known positions, previous times, and known frequency bands to perform the prediction in the

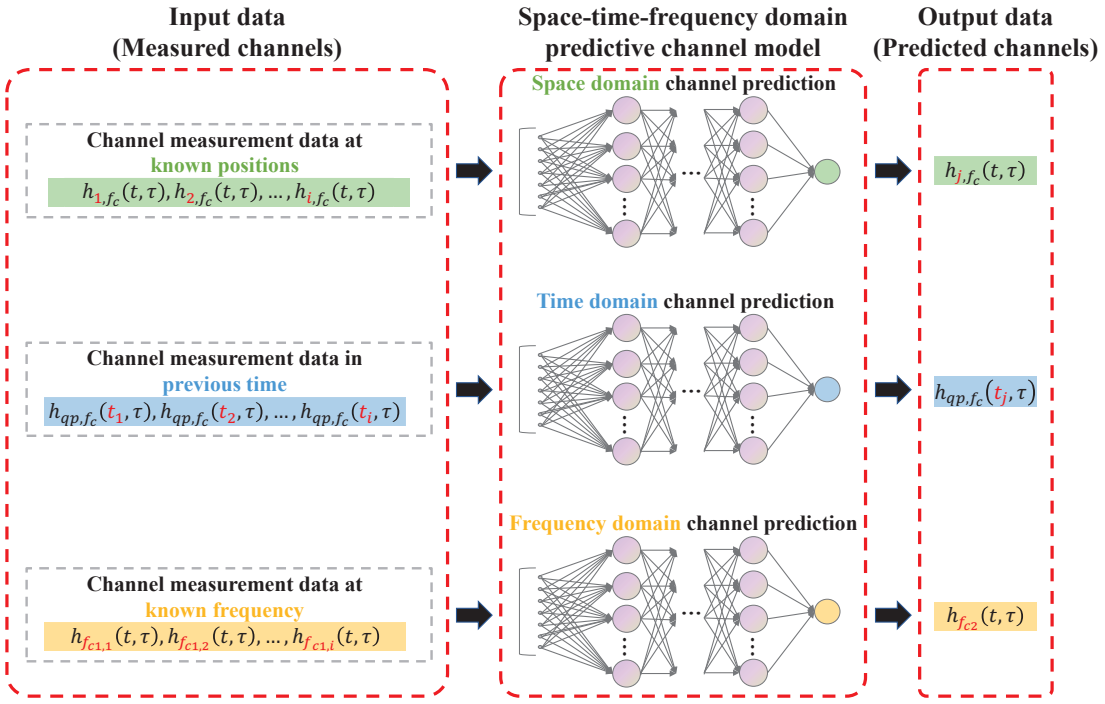

Fig. 1. The ML-based predictive channel modeling architecture in the space-time-frequency domains.

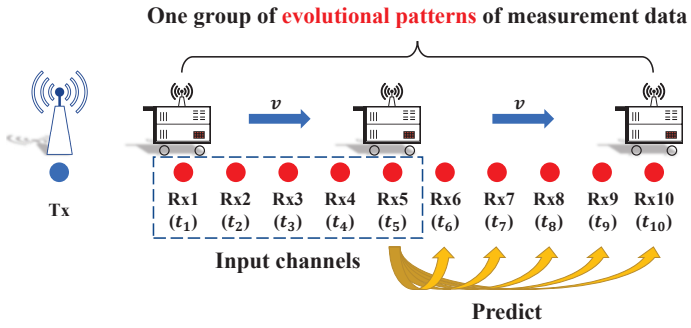

Fig. 2. The space-time characteristics of the channel.

space, time, and frequency domains, respectively. The pervasive predictive channel model is constructed based on multi-task learning ML algorithms, using common base layers to extract the common features of channels and then using some specialized layers (with distinct heads) to predict channels in different domains. Given the continuous nature of channels influenced by dynamic physical environmental properties in the space-time domains and the existence of frequency gaps between each frequency band, the space-time joint predictive channel modeling method becomes indispensable for achieving more accurate and comprehensive channel modeling.

Specifically, channel variations at several continuous spatial positions need to be accompanied by the temporal continuity of the channel. Channel modeling in the space-time domains needs to jointly capture an inherent dynamic trend of the space-time characteristics in the case of continuous channel variations, and this channel variation is called one group of evolution patterns of the channel data. As shown in Fig. 2, when the Tx is fixed, a group of continuous measurement data obtained by the movement of the Rx trolley from one position to another in a straight-line moving can only be used as one training data pattern to extract the channel space-time characteristics. Therefore, in order to construct a more accurate space-time joint channel model for this scenario, it is necessary to find as many continuous data patterns as possible to accurately capture the channel space-time variations and correlations, so a great amount of channel measurement data are required. In this work, based on the preliminary basic work in [34], a GAN-GRU based space-time joint predictive channel model is proposed to solve the challenges in channel measurement and modeling in the space-time domains for 6G communications. It can mine the inherent channel characteristics for efficient feature extraction and jointly predict unknown channel characteristics using known data in the space-time domains. The prediction problem can be expressed as:

$$\{h_{n,f_c}(t_n,\tau)\}_{n=1}^{i} \overset{\text{GAN-GRU}}{\Rightarrow} \{h_{m,f_c}(t_m,\tau)\}_{m=i+1}^{j} \quad (4)$$

where n means nth known positions in t_n, m means mth predicted positions in t_m. The details are explained in Section III.

III. A GAN-GRU Based Space-time Joint Predictive Channel Model

In this section, we will introduce the principle and architecture design of the GAN-GRU based predictive channel model. The architecture design of the GAN-GRU based joint predictive channel model is shown in Fig. 3. In the predictive channel model, the input $h_{1,f_c}(t_1,\tau)$, $h_{2,f_c}(t_2,\tau)$, $\cdots$, $h_{i,f_c}(t_i,\tau)$ are the channel measurement data at known positions and times from the 1st to the ith. The next module is the channel data augmentation module, using the STGAN to generate sufficient synthetic datasets with the space-time characteristics, for further channel prediction in the space-time domains. Then, to improve the prediction performance in the sequence-related channel data, a path identification

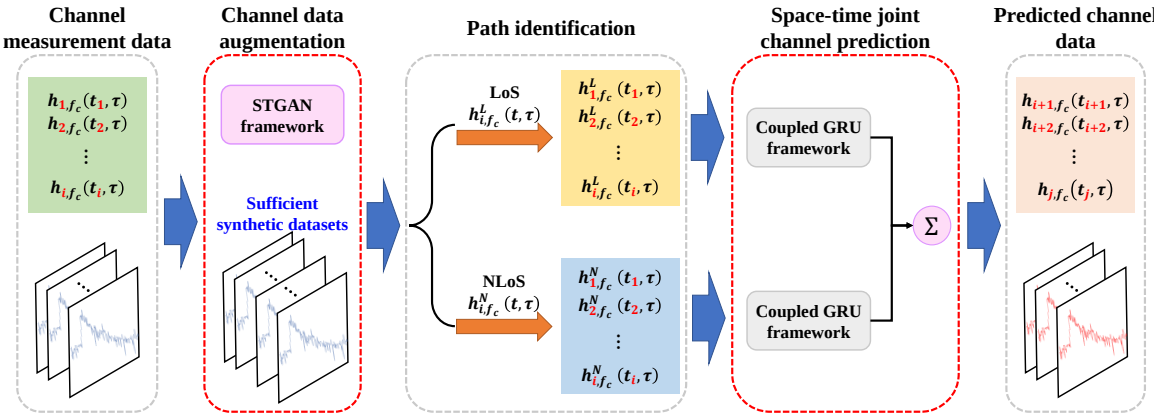

Fig. 3. The framework of the GAN-GRU based joint predictive channel model.

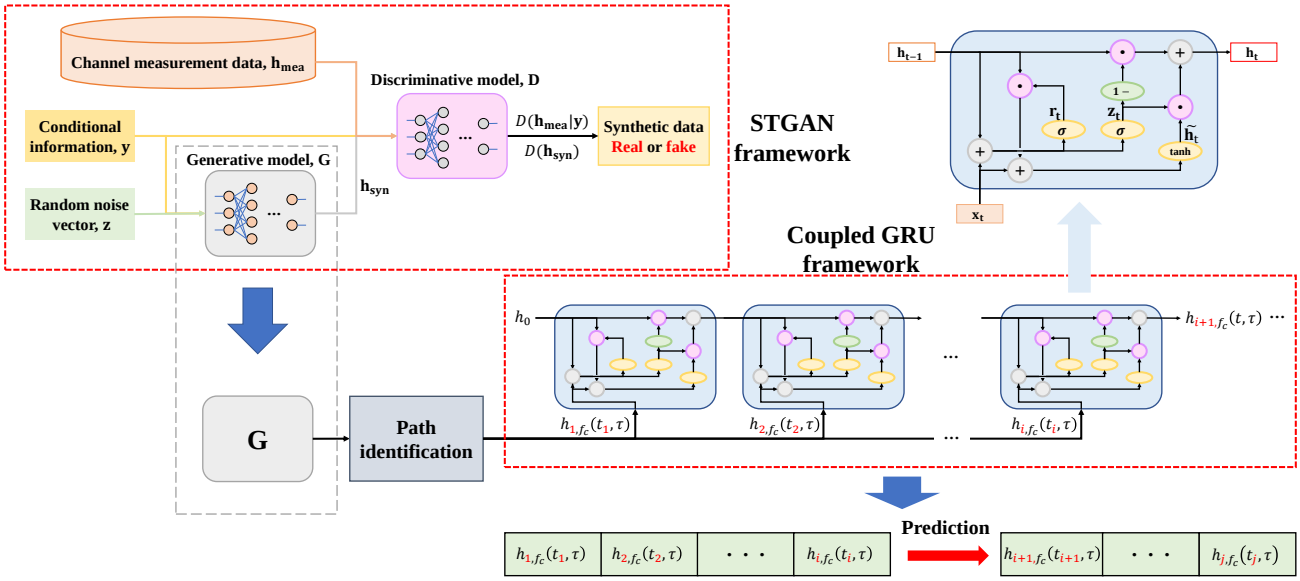

Fig. 4. The network structure of the GAN-GRU based joint predictive channel model.

module is used to classify channel data into LoS $h_{i,f_c}^{LoS}(t_i,\tau)$ or NLoS $h_{i,f_c}^{NLoS}(t_i,\tau)$ in the measured and synthetic channel data for better feature extraction. The GRU is used to capture the features of the input channel sequence from 1st to ith in LoS or NLoS scenarios to do the space-time channel prediction at unknown positions with time order. The outputs of the GRU in different paths are summed up to the predicted channels, which are the final predicted results $h_{i+1,f_c}(t_{i+1},\tau)$, $h_{i+2,f_c}(t_{i+2},\tau)$, ..., $h_{j,f_c}(t_j,\tau)$ in the space-time domains. The network structure of the GAN-GRU based joint predictive channel model is shown in Fig. 4 and is explained in more detail as follows.

A. Data Augmentation

The biggest challenge in ML-based predictive channel modeling is the lack of training data. Ray tracing (RT) can solve this issue by simulating channels in a site-specific manner [35]. However, it is hard by RT to obtain channel statistical characteristics due to the constant CIR, because the solutions to Maxwell's equations in the same ray optics scenario are fixed [36]. In addition, constructing a deterministic channel model using RT requires high computational complexity and resources. GAN, on the other hand, can be used for data augmentation [37] and has been proven to be a more accurate architecture for synthesizing channel data than variational auto-encoder and flow network [30]. Using GAN for channel data augmentation can provide more accurate channel models with the space-time characteristics and save computation resources and time by training offline. Therefore, GAN is a promising approach to obtaining sufficient channel data for wireless channel modeling.

The conditional GAN (CGAN) is an improvement made based on GAN by conditioning the model on additional information [48]. By adding additional conditional information to the generative model and discriminative model of the normal GAN, CGAN can better obtain synthetic data with oriented features. The proposed STGAN exploits the convolutional layers as the main structure with additional space-time information, which better captures the intricate channel characteristics than normal CGAN. The STGAN generates synthetic data similar to real data through adversarial learning of the two sub-models: the generative model G and the discriminative model D. The channel data augmentation can

be summarized in the following stepwise procedure:

Step 1 Collect and pre-process channel measurement data. CIR describes the effects of delay and fading experienced by the signal during multipath propagation, which is an essential characteristic for channel modeling [5]. CIR inherently contains both real and imaginary components, which provide a more comprehensive representation of the channel behavior. In the data augmentation module, the CIR collected from channel measurements can be denoted as $\mathbf{h_{mea}} = h_{qp,f_c}(t,\tau) \subseteq \mathbb{R}^{S\times N\times 2}$, where S means the number of CIR samples, N refers to the delay points in the delay domain, and 2 denotes the real and imaginary components of measured CIR. This integration of complex-valued CIR data enhances the accuracy and fidelity of the data augmentation process.

Step 2 Determine the channel large-scale and small-scale characteristics. Channel large-scale and small-scale characteristics are calculated from the measured CIR, which are used as conditional data $\mathbf{y}$ to guide the generation of synthetic channel data

$$\mathbf{y} = [PL(d), \tau_{DS}(d), K_R(t)] \tag{5}$$

where $PL(d)$ and $\tau_{DS}(d)$ refer to the PL and DS at different positions, respectively.

Step 3 Build the generative and discriminative models for the STGAN. The generative model takes a random Gaussian noise vector $\mathbf{z}$ and the conditional data $\mathbf{y}$ as input, and outputs synthetic data that mimic the real data to generate vectors $\mathbf{h_{syn}} = \mathbf{G}(\mathbf{z}|\mathbf{y})$. The discriminative model takes either channel measurement data $\mathbf{h_{mea}}$ or synthetic data $\mathbf{h_{syn}}$ and the corresponding conditional data $\mathbf{y}$ as input, and outputs a binary classification result $D(\mathbf{h_{mea}}|\mathbf{y})$ (i.e., whether the data is real or synthetic).

Step 4 Train the STGAN models using the collected channel measurement data. During training, the generative model G generates synthetic data with the same channel characteristics as the real data and the discriminative model D learns to distinguish them in a min-max game. The objective is to minimize the following loss function:

$$\mathcal{L}(D,G) = E_{\mathbf{h_{mea}}\sim P_{\mathbf{h_{mea}}}}[\log(D(\mathbf{h_{mea}}|\mathbf{y}))] + E_{\mathbf{z}\sim P_{\mathbf{z}}}[1-\log(D(\mathbf{h_{syn}}))] \tag{6}$$

where $E[\cdot]$ represents the expectation, $P_{\mathbf{z}}$ is the data distribution of the vector $\mathbf{z}$, and $P_{\mathbf{h_{mea}}}$ is the channel measurement data distribution. $D(\mathbf{h_{syn}})$ is the probability that D determines that the CIR generated by G is real based on condition $\mathbf{y}$.

Step 5 Evaluate the models. After training, evaluate the performance of the generative and discriminative models by testing their ability to generate synthetic CIR that resembles the measured CIR in terms of channel space-time characteristics. The discriminative ability of D converges to the optimum value D_G^* as

$$D_G^* = \frac{P_{\mathbf{h_{mea}}}}{P_{\mathbf{h_{syn}}} + P_{\mathbf{h_{mea}}}} \tag{7}$$

where $P_{\mathbf{h_{syn}}}$ is the data distribution of the synthetic CIR. As $P_{\mathbf{h_{syn}}}$ approaches $P_{\mathbf{h_{mea}}}$, D_G^* approaches 0.5. In this case, D is unable to distinguish between the real channel data and the synthetic channel data.

Step 6 Once the models converge after fully learning the space-time characteristics of the channel measurement data, the generative model can be cut from the STGAN to independently generate synthetic channel data. These synthetic data can be used to supplement the real data and improve the accuracy of joint channel prediction in the space-time domains.

B. Path Identification

The main difference between channels with typical space-time characteristics at different spatial positions is manifested in large-scale fading and small-scale fading. The LoS path of the channel can clearly show large-scale fading, while there is small-scale fading caused by multipath effects in the NLoS path. In practical applications, accurate identification of the LoS path and NLoS path can eliminate the negative impact of errors on the channel and can greatly improve the efficiency of data processing and extract the channel characteristics of the corresponding multipath information [39]. Therefore, in order to effectively improve the channel prediction performance in the space-time domain, the channel is identified and classified into LoS path and NLoS path based on the CIR statistical characteristics and the received power. Then, the processed data are sent independently to the GRU model for feature extraction and prediction.

According to (1), (2), and (3), the wireless channels deliver significantly different characteristics in the LoS and NLoS paths. The path identification module uses the delay power spectral density (PSD) obtained from the CIR to identify the LoS/NLoS paths, as shown in the following expression:

$$S_{qp,f_c}(t,\tau) = |h_{qp,f_c}(t,\tau)|^2 \tag{8}$$

A threshold exists so that the delay PSD $S^L_{qp,f_c}(t,\tau)$ of the LoS path and the delay PSD $S^N_{qp,f_c}(t,\tau)$ of the NLoS path can be identified and classified. The delay PSD-based LoS/NLoS path identification algorithm is shown in Algorithm 1.

C. Space-time Joint Channel Prediction

GRU and LSTM are RNNs with time-step, which are suitable for processing and predicting data with sequence-related characteristics [40]. They are designed to solve the long-term dependence problem of the RNN by introducing a gate mechanism to control the transmission of information. Considering the convergence in CPU time, parameter updates, and generalization, GRU is better than LSTM due to its more efficient structure [41]. One of the important characteristics of GRU is that the sequence-related data prediction in the network is processed by time-step, such as using previous states to predict current or future states, which effectively solves the problems of vanishing or exploding gradients. To jointly predict the space-time channel characteristics, the channel prediction is represented as a sequence-related prediction problem with space-time steps. Thus, several coupled GRUs

Algorithm 1: The Delay PSD-Based Path Identification Algorithm.

Parameters: The length of $S_{qp,f_c}(\tau)$ in the delay domain, Len. The width of delay segmentation for $S_{qp,f_c}(\tau)$ in the delay domain, W. The width of overlap between adjacent intervals for $S_{qp,f_c}(\tau)$ in the delay domain, $ovlp$. The threshold for peak value of $S^L_{qp,f_c}(\tau)$, T_1. The threshold for average value of $S^L_{qp,f_c}(\tau)$, T_2;

Input: The delay PSD of $S_{qp,f_c}(\tau)$;

Output: The result array, $Result$;

for i in range $(0, Len - W + 1, W - ovlp)$ **do**

  if $i + W > Len$ **then**

    break;

  else

    $S(i) = S_{qp,f_c}(i : i + W)$;

    $\hat{S}(i) = max\{S(i)\}$;

    $\bar{S}(i) = mean\{S(i)\}$;

    if $i + W > Len$ **then**

      $Result[i]$ =“LoS”;

    else

      $Result[i]$ =“NLoS”;

    end

  end

end

Calculate the peak and mean values of the first and last delay intervals using the overlap between adjacent intervals, and output the final identification result;

Perform post-processing on the $Result$ array based on the peak and mean values to correct some intervals that were incorrectly identified as NLoS paths;

are used to construct the GRU framework for the space-time joint channel prediction.

When antenna position routes are deployed in a straight line, the prediction method uses the k previous CIRs obtained by continuous measurements to predict the next channel CIR in the space-time domains, as demonstrated in Fig. 5. When the sequence-related channel data obtained at the continuous Rx positions are used as the input, the GRU model conducts unknown position prediction by learning from information at the previous positions. The output of the GRU model, $\mathbf{h_t}$, includes the time-step updated information obtained from the CIR sequences as

$$h_{i,f_c}(t,\tau) = \arg \max_{h_{i,f_c}(t_i,\tau)} p(h_{i,f_c}(t_i,\tau) \mid h_{i-k+1,f_c}(t_{i-k+1},\tau), h_{i-k+2,f_c}(t_{i-k+2},\tau),\cdots,h_{i-1,f_c}(t_{i-1},\tau)) \tag{9}$$

$$h_{i+1,f_c}(t_{i+1},\tau) = h_t = f_{GRU}(h_{i-k+1,f_c}(t_{i-k+1},\tau), h_{i-k+2,f_c}(t_{i-k+2},\tau),\cdots,h_{i,f_c}(t_i,\tau)). \tag{10}$$

The GAN-GRU based joint predictive channel model not only has the ability to conduct data augmentation by GAN to generate corresponding channel datasets with the space-time characteristics but also extracts sequence data features by GRU to do joint prediction in the space-time domains.

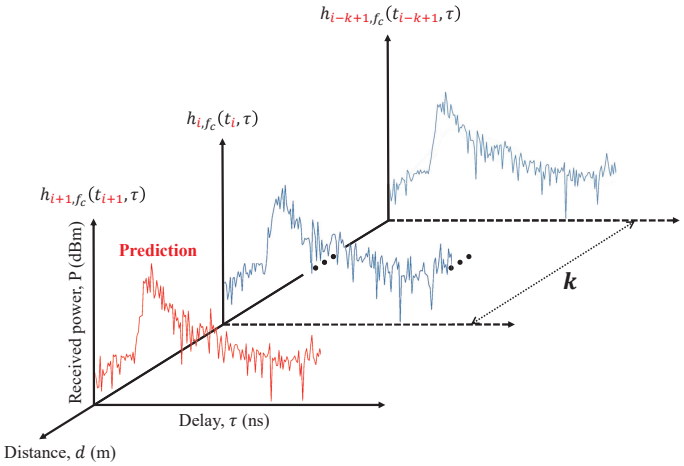

Fig. 5. The space-time joint channel prediction by GRU.

IV. Channel Measurements and Algorithm Implementation

In this section, we will first introduce the channel measurement dataset for prediction experiments and then describe the data and network pre-processing used in experiments. We will also discuss the algorithm implementation of the GAN-GRU based joint predictive channel model. Finally, the criteria are introduced to evaluate the channel prediction performance.

A. Channel Measurement Dataset

The indoor corridor is a typical scenario containing space-time channel characteristics [42], thus the channel measurement data used for validation was conducted at 2.4 GHz, 5 GHz, and 6 GHz frequency bands in an indoor corridor scenario [43]. The bandwidth at each center frequency is 320 MHz. Configurations about the channel sounder are listed here: the delay resolution is 3.125 ns, the length of pseudo-noise sequences is 4800, and the maximum output power is 20 dBm. This multi-frequency channel measurement campaign was performed by one Tx and one Rx, where the Tx and Rx antennas were placed on the trolley to change positions during measurement. Besides, the Tx antenna height is 1.95 m and the Rx antenna height is 1.45 m.

According to the distribution of antennas, the channel measurement under this corridor can be divided into two scenarios: LoS and NLoS. The position of Tx and Rx antennas can be seen in Fig. 6, where the blue dots represent the positions of Tx and the red dots represent the positions of Rx. When conducting channel measurement in the LoS scenario, Tx was located at position Tx1. In this scenario, Rx moved from position Rx1 to position Rx37, and the interval between every two positions from position Rx1 to position Rx17 is 0.8 m, 1.6 m from position Rx18 to position Rx37. When conducting channel measurement in the NLoS scenario, Tx was located in position Tx2, where the positions of Rx only include the 34 points from position Rx4 to Rx37, and the other configurations are the same as in the LoS scenario.

B. Data Pre-Processing

When obtaining CIR by indoor corridor measurements, the response of the measurement system changes very slowly. It

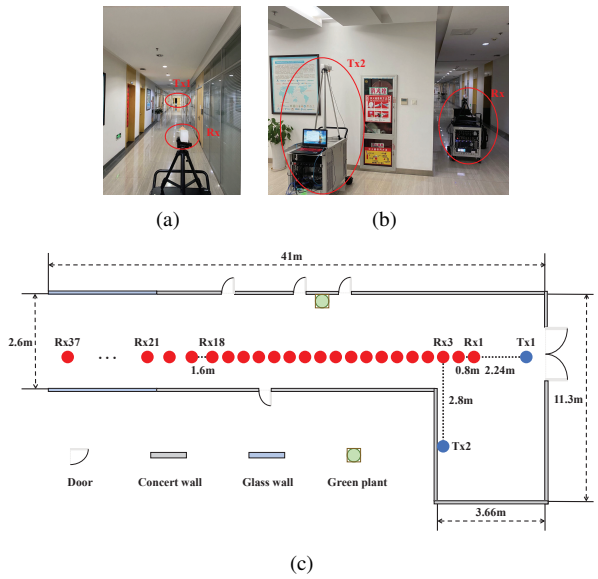

Fig. 6. The indoor corridor channel measurement campaign: (a) LoS scenario, (b) NLoS scenario, and (c) Layout and antenna positions of the corridor.

can be broadly defined as a time-invariant system. Besides, the channel coherence time is much greater than the duration of each snapshot during the measurement. Thus, the CIR of each snapshot can also be regarded as time-invariant. Given that the transmitter and receiver were stationary or had minor movement without high speed during each data point collection, the Doppler effect is not considered in this work. To enhance the accuracy of the measurement data, outliers are removed to ensure that the remaining snapshots are highly correlated using the snapshot correlation method in [44]. Additionally, a multipath power decision threshold is used to eliminate errors [45], which is determined by selecting the higher value between the noise floor plus 6 dB and the maximum power minus 25 dB.

When using neural networks for training and learning channel data, the input dataset needs to be normalized. Normalization is a data pre-processing method to resist outliers to make them relatively stable and suitable for noisy data scenarios. In order to characterize the channel small-scale parameters and capture the channel small-scale characteristics in the modeling process, this paper uses the power normalization method proposed in the 3GPP TR 38.901 standardized channel model [46]. Supposing the sum of all path powers is equal to 1, the power of the delay PSD is normalized by dividing the total power in the current delay domain, and the normalization method is expressed as

$$P_N(t,\tau) = \frac{P(t,\tau)}{\sum_{l=1}^{L} P_l(t,\tau)} \tag{11}$$

where $P_N(t,\tau)$ is the nomalized power, $P(t,\tau)$ is the received power of delay PSD, $P_l(t,\tau)$ represents the power of the lst path, and L represents the total number of paths. The normalized real-value data are fed into the proposed GAN-GRU network for data augmentation and the space-time prediction. Normalization does not change the information but only transfers its representation into the range [0, 1] to speed up the convergence of the training network. Finally, the output is denormalized, and the power is taken logarithmically to transform the linear power (w) into log-domain power (dBm).

TABLE I
THE PARAMETERS OF THE GENERATIVE MODEL.

Layers	Model parameters
Conv1	kernel size: 5×5, stride: 2, padding: 2
BN1	feature number: 32
Conv2	kernel size: 5×5, stride: 2, padding: 2
BN2	feature number: 16
Conv3	kernel size: 5×5, stride: 2, padding: 2
BN3	feature number: 8
Conv4 + tanh	kernel size: 5×5, stride: 2, padding: 2

C. Implementation

In this part, we implement the proposed channel model mentioned in Section III. Since the STGAN generative model cannot obtain the real channel data distribution, it is not necessary to be constructed with too sophisticated architectures. The reason is that although an overly complex model may generate synthetic data with channel characteristics, it complicates the learning process and increases the time consumption and computational resources. According to training experience, using a specific training method for a specific data type is an important reference index for optimizing the model. Therefore, the convolutional (Conv) layer is used as the main structure for its good recognition performance on high-dimensional matrices and complex features. By using the pre-training of the different numbers of Conv layers in this model, four Conv layers have a better trade-off between prediction accuracy and time consumption than three or five Conv layers. Besides, the function of the batch normalization (BN) layer added after the Conv layer is to normalize the outputs of each node of the layers to enhance the generalization and robustness of the model. After that, the parametric rectified linear unit (PReLU) activation function is used for non-linear reprocessing to improve the accuracy and efficiency of training. Finally, the tanh layer is used for non-linear transformation. The parameters of the generative model are shown in Table I.

The discriminative model needs to know the distribution of feature points of the real channel data, so the construction of the discriminative model should be more sophisticated than the generative model. In the discriminative model of the STGAN, five Conv layers and one fully connected (FC) layer are used for network construction. Like the Conv layers in G, the Conv layers in D are used to extract the multi-dimensional features of the sequence data for prediction. In addition to the BN layer and PReLU, the Dropout layers are added to the D model, which can improve the overfitting resistance of the neural network and enhance its generality. In the preliminary experiment of the pre-trained network, the dropout ratio of the dropout layer, ranging from 0 to 1, is analyzed for the impact on the accuracy of this predictive channel model, and the dropout ratio of 0.4 has the best prediction result. Finally,

TABLE II
THE PARAMETERS OF THE DISCRIMINATIVE MODEL.

Layers	Model parameters
Conv1	kernel size: 3×3, stride: 2, padding: 0
BN1	feature number: 8
Conv2	kernel size: 3×3, stride: 2, padding: 0
BN2	feature number: 16
Conv3	kernel size: 3×3, stride: 2, padding: 0
BN3	feature number: 32
Conv4	kernel size: 3×3, stride: 2, padding: 0
BN4	feature number: 64
Conv5	kernel size: 3×3, stride: 2, padding: 0
BN5	feature number: 128
FC + Sigmoid	input channel: 128, output channel: 1

an extra FC layer and Sigmoid layer are added to get better learning efficiency for discrimination. The parameters of the discriminative model are shown in Table II.

The training process of the proposed predictive channel model is demonstrated in Algorithm 2. The GRU network has two hidden layers, each with 256 units, where the PReLU activation function is used for the hidden layers. Besides, several hyper-parameters are also tuned to increase the performance of prediction. The weights of the proposed model are updated by Adam optimizer [47] with a β_1 value of 0.5 and a β_2 value of 0.999 to avoid overfitting. The batch size is set to 128, and we train the model for 2500 epochs with an initial learning rate of 0.0001 and a learning rate decay of 0.9. When considering the prediction performance of the GRU, the parameter k is an important hyper-parameter related to channel memory and will be studied in the experiment in Section V.

Algorithm 2: The training Algorithm of the GAN-GRU Based Predictive Channel Model.

Parameters: The learning rate of D, α_D. The learning rate of G, α_G. The batch size, m. The number of iterations of D per G, n. The previous states learned by GRU, k;

Initialization: The parameter of D, θ_D. The parameter of G, θ_G;

for *number of training iterations* **do**

  for t = *0, 1,* $\cdots$, n **do**

    Sample batch from the real data, $\{h_1, h_2, \cdots, h_m\} \sim P_{\mathbf{h_{mea}}}(\mathbf{h_{mea}})$;

    Sample batch from the noise prior, $\{z_1, z_2, \cdots, z_m\} \sim P_{\mathbf{z}}(\mathbf{z})$;

    Update the discriminative model: $g_{\theta_D} = \bigtriangledown_{\theta_D}[\frac{1}{m}\sum_{i=1}^{m} logD(h_i|\mathbf{y}) + \frac{1}{m}\sum_{i=1}^{m} log(1 - D(z_i|\mathbf{y}))]$;

    $\theta_D = \theta_D - \alpha_D \cdot Adam(g_{\theta_D}, \theta_D)$;

  end

  $g_{\theta_G} = \bigtriangledown_{\theta_G}[\frac{1}{m}\sum_{i=1}^{m} log(1 - D(G(z_i|\mathbf{y}))]$;

  $\theta_G = \theta_G - \alpha_G \cdot Adam(g_{\theta_G}, \theta_G)$;

end

Cut the generative model for the converged STGAN and attach it to the GRU;

Sample batch generated from the generative model, $\mathbf{h_{syn}} = \{G(z_i|\mathbf{y})\}_{i=1}^{m}$;

Total sample batch, $\hat{\mathbf{h}} = \left\{\hat{h}_i\right\}_{i=1}^{m} = \{\mathbf{h_{mea}},\ \mathbf{h_{syn}}\}$;

Predicted data from the GRU: $h_t^{i+1} = f_{GRU}(\hat{h}_{i-k+1}, \hat{h}_{i-k+2}, \cdots, \hat{h}_i)$.

V. RESULTS AND ANALYSIS

In this section, the space-time joint channel prediction experiments are conducted at 2.4 GHz, 5 GHz, and 6 GHz in LoS and NLoS scenarios in the indoor corridor to verify the prediction performance of the proposed channel model. First, comparative experiments with existing data augmentation methods are conducted to show the effectiveness and gain of the synthetic channel data by the proposed model. After that, the value of parameter k related to the channel memory in the space-time joint channel prediction is analyzed by experiments. Then, channel statistical properties of the channel data generated by the proposed model and 6GPCM are compared to validate the proposed model. In addition, the comparison between the proposed model and the existing ML-based methods is conducted on two kinds of datasets for performance evaluation. Finally, the proposed model is further validated in the outdoor channel measurement dataset to show its generality.

A. Channel Data Augmentation Performance

It is time-consuming and labor-intensive to collect channel measurement data, resulting in insufficient training data, which ultimately affects the accuracy of the channel space-time joint prediction. To ensure that there are a sufficient amount of data during training and that the dataset has the same channel space-time characteristics as the measurement data, we use the STGAN to do data augmentation. The similarity and diversity [30] are exploited to evaluate the effectiveness and gain of the augmented channel data from the perspective of feature similarity and diversity. For each type of channel, the similarity between the distribution of the synthetic channel dataset and the channel measurement dataset is evaluated as

$$\mathfrak{S} = \frac{1}{N_{syn}} \sum_{N_{syn}}^{u=1} \max_{1 \ll v \ll N_{mea}} \frac{\left\|h_u^H h_v'\right\|^2}{\left\|h_u\right\|^2 \left\|h_v'\right\|^2} \tag{12}$$

where $\|\cdot\|$ represents 2-norm operation, N_{syn} represents the number of synthetic CIRs, and N_{mea} represents the number of measured CIRs. h_u and h_v' refer to the vectorized uth synthetic channel data $\mathbf{h_{syn}}$ and vth channel measurement data $\mathbf{h_{mea}}$, respectively.

The diversity of the synthetic channel is evaluated by

$$\mathfrak{D} = \sqrt{Var(\mathbf{l})} \tag{13}$$

where $Var(\cdot)$ calculates the variance of the input vector. The element l_k of $\mathbf{l} = [l_1, l_2, ..., l_{N_{mea}}]$ shows the multiplexity of the synthetic channel, and is defined as

$$l_k = count(\arg \max_{1 \ll v \ll N_{mea}} \frac{\left\|h_u^H h_v'\right\|^2}{\left\|h_u\right\|^2 \left\|h_v'\right\|^2} = k) \tag{14}$$

TABLE III
THE COMPARATIVE RESULTS BETWEEN DIFFERENT DATA AUGMENTATION METHODS.

	STGAN	GAN	DCGAN	WGAN
Similarity $\mathfrak{S}$	0.4888	0.1857	0.2740	0.4372
Diversity $\mathfrak{D}$	1.4259	4.8211	3.3135	2.1478

where $count(\cdot)$ denotes the total number of the synthetic data which is most similar to the kth channel measurement data.

To evaluate the effectiveness of the proposed STGAN in synthesizing channel data, comparative experiments are conducted against existing data augmentation methods, including normal GAN [26], deep convolutional GAN (DCGAN) [48], and Wasserstein GAN (WGAN) [49]. The experiments involved synthesizing channel data using each method and comparing the results in terms of data similarity and diversity by criteria (12) and (13). Specifically, the ability of these methods to produce CIR is evaluated to show that they accurately capture the complex space-time characteristics of wireless channels, including variations in received power, delay, and spatial distributions.

According to Table III, the results of the comparative experiments demonstrated that the proposed STGAN has better performance in terms of CIR similarity and diversity than normal GAN and DCGAN. The primary reason for this superior performance is the incorporation of space-time channel characteristics as conditional inputs to synthesize CIRs that closely align with the measured CIRs. By conditioning the generative model on specific channel characteristics and extracting features based on CNN structure, the STGAN can better capture the inherent complexity of wireless channels. Moreover, while WGAN is more concerned with the optimization of the Wasserstein distance metric and can improve training stability in CIR similarity, it may not achieve the same level of data diversity as STGAN when generating complex data in different spatial positions and time series. The three-view visualization comparison of the measured channel and synthetic channel at 2.4 GHz is shown in Fig. 7, where STGAN generates the synthetic data based on the normalized channel measurement data. The total datasets including measurement data and synthetic contain 213,000 CIRs at each Rx position, where each frequency band in different LoS or LoS scenarios includes 1,000 CIRs. The datasets are sufficiently shuffled to ensure that the test and training sequences do not have any overlap and split into 80% for training and 20% for testing. The proposed model is trained on the training set and the optimal network is used for evaluation on the test set.

B. Channel Prediction Performance with Different Channel Memory Parameters

To analyze the impact of channel memory parameters k on the space-time joint predictive channel modeling, the proposed models with different values of k are used to reconstruct the indoor corridor channels and predict channels at unknown positions and times. By comparing the channel prediction performance, the optimal channel memory parameter is determined

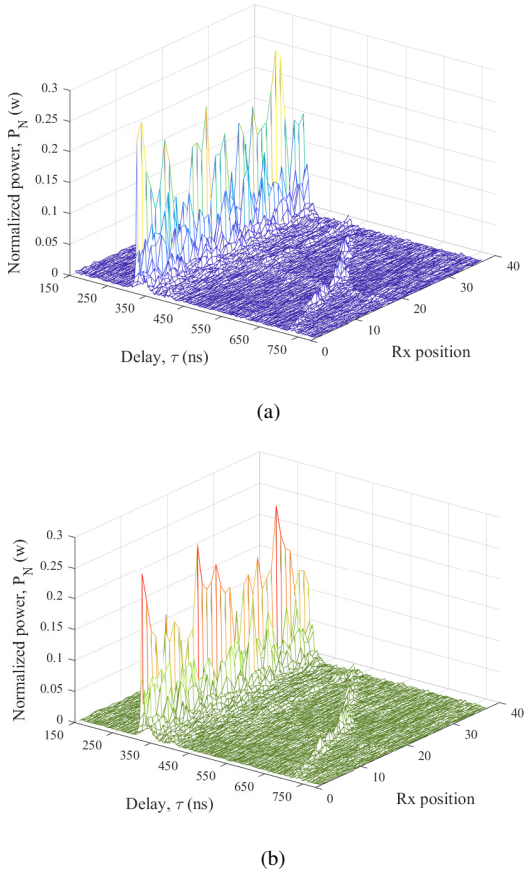

Fig. 7. The three-view visualization comparison of the real channel and synthetic channel at 2.4 GHz: (a) real channel from channel measurement, and (b) synthetic channel trained for 2500 epochs.

for further study. In this indoor corridor with typical space-time characteristics, the total number of antenna positions is no more than 37. Therefore, when conducting CIR prediction at unknown positions, the number of previous CIRs k must be determined in a specific range.

As the complex CIR contains both magnitude and phase information, representing channel space-time joint characteristics using the real-valued average delay PSD is more intuitive compared to the complex-valued CIR. Therefore, RMSE is preferred as a metric for evaluating prediction performance using the real-valued average delay PSD. It provides a more meaningful measure of prediction accuracy in this context.

$$RMSE = \sqrt{\frac{1}{n}\sum_{i=1}^{n}[S_{pred}(i) - S_{mea}(i)]^2} \qquad (15)$$

where n is the delay dimension, S_{pred} is the predicted delay PSD, and S_{mea} is the actual measured delay PSD.

The RMSEs of the proposed predictive channel models with different k are shown in Fig. 8. It can be seen from the figure that when k is less than 8, the RMSEs are larger as k decreases because the effective feature extracted from the channel space-time characteristics is not sufficient to feed into the GRU for channel prediction. When k is more than 8, some channel information with low correlation is aggregated,

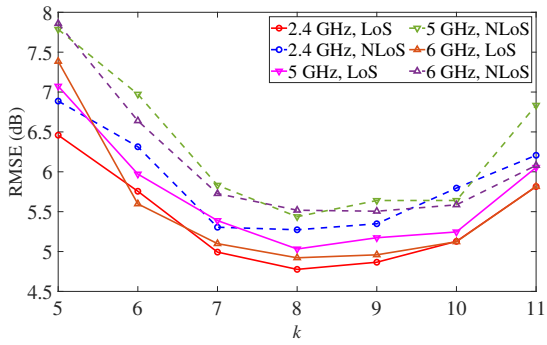

Fig. 8. The RMSEs of the proposed predictive channel models with different k.

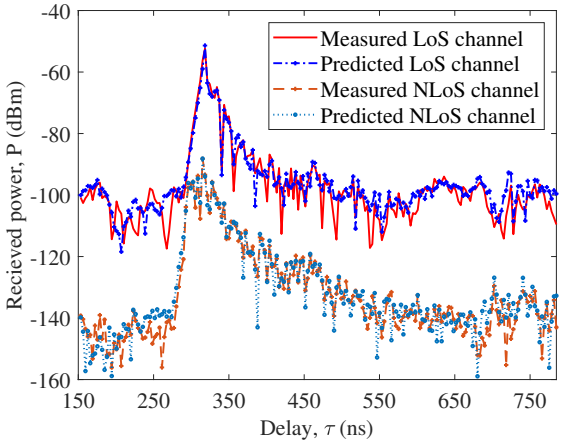

Fig. 9. The average delay PSD of measured channels and predicted channels in LoS and NLoS scenarios at 6 GHz.

leading to overfitting in the training sets and thus degrading the performance in the test set. When the channel memory parameter k is set to 8, the corresponding predictive channel model has the best prediction performance with the least RMSE.

Fig. 9 shows the average delay PSDs of channels at 6 GHz, where the predictive channel model uses the optimal value of the channel memory parameter. It can be seen that the proposed model has achieved good joint prediction results in the indoor corridor LoS and NLoS scenarios, where the received power of the predicted channel matches well with the received power of the measured channels. Most dominant paths are successfully predicted with negligible error. The multipath effect of the wireless channels in the indoor corridor is well illustrated in the predicted channels by GAN-GRU because of the efficient and accurate structure of coupled GRUs to capture the sophisticated space-time joint characteristics. Moreover, the prediction accuracy in LoS scenarios is generally higher than that in NLoS scenarios because the average received signal power of the LoS channels is higher than that in the NLoS channels. The greater the ratio of received power to noise, the greater the proportion of useful features extracted during the ML training process, and therefore, the closer the results of the predicted channel model are to the actual channel model. The same observation can be made for 2.4 GHz and 5 GHz. Therefore, the above observation demonstrates that the proposed model with the optimal value of k can capture the large-scale fading difference with channel space-time characteristics.

C. Channel Statistics Properties Analysis

In this part, the relationships between the statistical properties generated by the measured channels and predicted channels are analyzed. A pervasive GBSM 6GPCM [33] integrating important channel characteristics at different frequency bands and scenarios is utilized to be compared to validate the proposed predictive channel model. The GAN-LSTM based predictive channel model proposed in [34] is also used for comparison. The delay PSD and RMS DS are used to analyze the system performance of the predictive channel model in the space-time domains, where delay PSD is a good representation of the multipath effect in the space domain and RMS DS is an indicator to reflect the time domain.

1) Delay PSD: Delay PSD is used to show the multipath effect of the indoor corridor channel with the space-time characteristics. Delay PSDs of measured, predicted, and 6GPCM simulated channels in different scenarios at 5 GHz are illustrated in Fig. 10. It can be seen that the delay PSDs of the predicted channels have a path with the strongest power, and the power of this path decreases as the distance between Tx and Rx increases. The delay of the reflection path that curves from the bottom to the top decreases as the distance between Tx and Rx increases due to the glass reflection at the bottom of this corridor. Moreover, during channel measurement campaigns, some antenna positions did not receive signals due to the sudden appearance of unavoidable obstacles or problems with the measurement equipment. As can be seen from Figs. 10 (a) and (e), at 5 GHz, the Rx11 and Rx16 positions in the LoS scenario and the Rx10 in the NLoS scenario have no values due to the error of measurements. The situation is the same at 2.4 GHz and 6 GHz. Through joint predictive channel modeling in the space-time domains, the proposed model can provide synthetic data to rebuild the lost channel measurement data, which have corresponding received power at these Rx positions with similar channel characteristics. Besides, compared with predicted channels by GAN-LSTM, delay PSDs predicted by GAN-GRU have better performance on the space-time domain prediction. This is because STGAN has a stronger ability to synthesize the same space-time channel data than normal GAN, which provides more sufficient and similar channel data for joint prediction. Besides, the coupled GRU framework has a shorter processing time and higher accuracy and is suitable for joint predictive channel modeling problems with obvious space-time sequence characteristics. It is also proven that 6GPCM simulated delay PSDs shown in Figs. 10 (d) and (h) have bigger differences from measurement data than the prediction data. The 6GPCM, as a pervasive GBSM, can effectively characterize channel statistical properties at all frequency bands and scenarios. However, its reliance on stochastic functions and parameter fitting introduces complexity to the channel modeling process. The adjustment and fitting of parameters to match measurement data can be challenging and may lead to overfitting or biases in the model. Moreover, the 6GPCM lacks strong

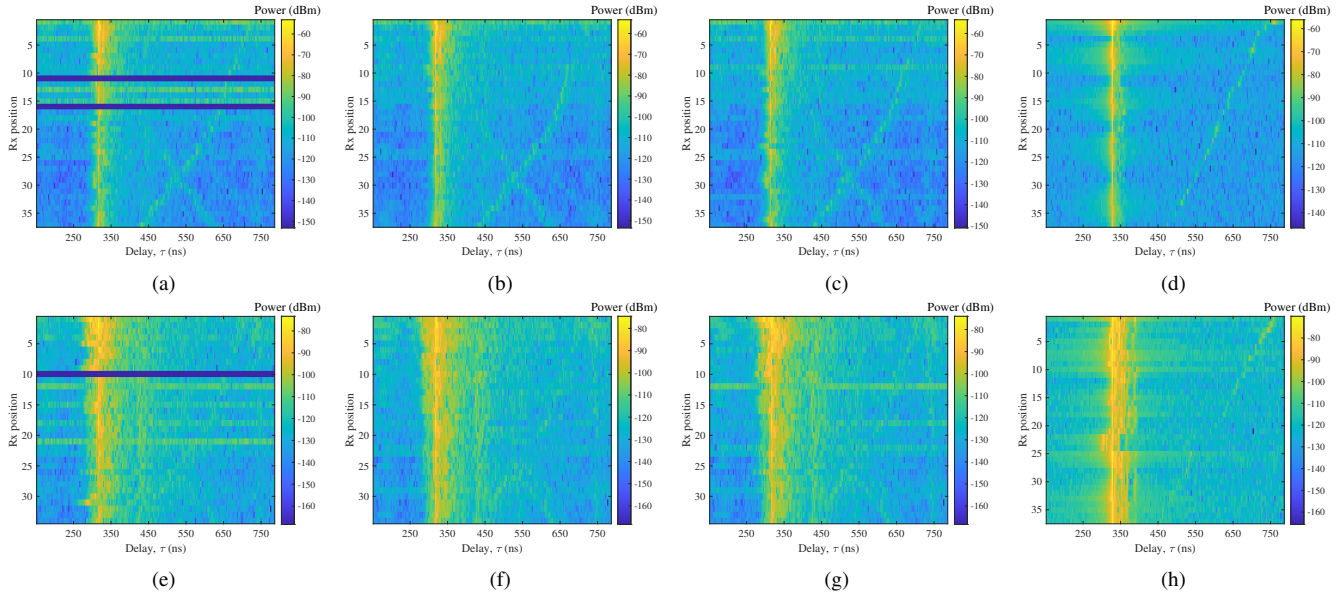

Fig. 10. The delay PSDs of measured, predicted, and 6GPCM simulated channels at 5 GHz: (a) LoS measurement data, (b) LoS prediction data by GAN-GRU, (c) LoS prediction data by GAN-LSTM, (d) LoS simulation data by 6GPCM,(e) NLoS measurement data, (f) NLoS prediction data by GAN-GRU, (g) NLoS prediction data by GAN-LSTM, and (h) NLoS simulation data by 6GPCM.

predictive capabilities for unknown scenarios or future channel variations based on limited channel data, especially when compared to ML-based modeling methods. This limitation arises from its inability to adequately capture the complex non-linear behavior of wireless channels.

Due to the influence of some environmental factors, human factors, and channel sounder system errors during measurement campaigns, CIR is affected by noise in certain delay periods, where CIR is far from the actual channel distribution characteristics. The proposed model can eliminate the abnormal data of the delay PSDs in the delay domain, thereby compensating for data that is more similar to the channel distribution in the actual scenario. As shown in measured channels, some strange yellow stripes are deeper than the surrounding colors, indicating that there is abnormal noise power. Besides, the path with the strongest power is presented as a zigzag line in the measured figures, which also demonstrates that there is some error during the channel measurement campaigns. However, the predicted figures illustrate that the abnormal color blocks are much fewer and the path is more accurate, which means that the abnormal data in the measurement has been corrected. The abnormal data-correction ability of GAN-GRU is better than that of GAN-LSTM due to the structures of STGAN and coupled GRUs for sequence-related data synthesizing and prediction. Moreover, GBSM-based simulated channels have larger deviations than the channels predicted by the proposed model. Therefore, according to the evaluation results, the proposed predictive channel model can accurately extract the channel space-time characteristics and jointly predict accurate channel data at unknown positions and times to rebuild the lost measurement data and correct the error, which improves the usability and accuracy of the channel data.

2) RMS DS: RMS DS is used to represent the time domain dispersion properties of wireless channels. The larger the RMS DS is, the more serious the dispersion in the time domain will be. As shown in Fig. 11, the cumulative distribution functions (CDFs) of DS at three frequency bands in LoS and NLoS scenarios are used to demonstrate the DS characteristics. Due to the insufficient measurement data, the curves of measured DSs at different frequency bands are bumpy. So they are needed to fit the results by the lognormal distribution method to show the actual DS distribution. It can be seen from these figures that the predicted DS curves using two predictive channel models match well the measured DS curves by lognormal fitting. Therefore, it is proved that the channels predicted by the proposed models can not only synthesize sufficient channel data to fit the actual propagation without extra lognormal fitting but also efficiently and accurately predict the unknown information in the space-time domains. Moreover, the DSs predicted by GAN-GRU are better than that predicted by GAN-LSTM. The predicted DSs in the LoS scenarios by these two predictive models are slightly worse than those in NLoS scenarios. Due to a strong reflection path in the LoS scenario, the delay of this reflection path is much longer than the delay of the LoS path, while its power is comparable to that of the LoS path, which makes the mean value of DS in LoS scenario greater than that in NLoS scenario. When doing feature extraction by ML, the power of the strong reflection path is comparable to the LoS path and has a negative impact on the DS prediction performance in LoS scenarios.

D. Prediction Performance Comparison

In order to further evaluate the prediction performance, the proposed GAN-GRU based model is compared with the existing ML-based methods GRU [41], LSTM [20], and RBF-NN [19]. In this part, two different datasets are used. One is the continuous space-time channel datasets used in space-time joint prediction experiments, and the other is the discrete

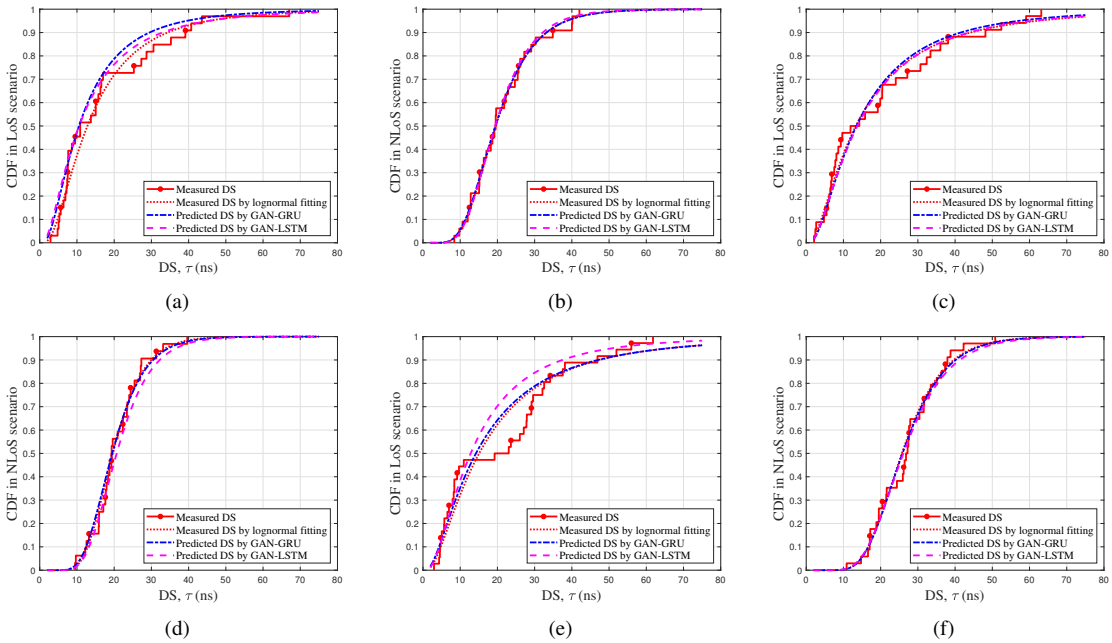

Fig. 11. The DSs of measured channels and predicted channels in different frequencies and scenarios: (a) 2.4 GHz, LoS, (b) 2.4 GHz, NLoS, (c) 5 GHz, LoS, (d) 5 GHz, NLoS, (e) 6 GHz, LoS, and (f) 6 GHz, NLoS.

channel parameter datasets with the total received power at each position in the corridor scenario.

1) Prediction Comparison on Continuous Space-time Channel Datasets: In the comparison, the network structures and dataset implementation of LSTM and GRU remain the same as those in the former framework, but the STGAN is removed, which means that the normal GRU model and LSTM model learn the features based on the limited original channel measurement data without the GAN's data augmentation.

Table IV gives the predicted delay PSDs in terms of RMSE and MAPE in different frequency bands and scenarios, where the results are the optimal values after using the Monte Carlo method. The error between 6GPCM simulated delay PSDs and channel measurement data is also shown in this Table. According to the comparison, the prediction accuracy of GAN-GRU is the best among the four networks, where the most accurate prediction results are highlighted in bold. GAN-LSTM is inferior to GAN-GRU, the prediction accuracy of GRU is better than that of LSTM and the 6GPCM simulation results are the worst. This is because the normal GRU and LSTM can only extract limited features in the insufficient channel measurement datasets, and the prediction results cannot reflect the whole channel characteristics by using regression algorithms without full training, especially in joint predictive channel modeling problems in the space-time domains. The advantage of STGAN is that it can perform data augmentation and generate a large amount of channel data for network training, which can effectively solve the problem of less measurement and simulation data in conventional channel modeling. Although the 6GPCM is an outstanding GBSM, it still relies on stochastic functions to generate channel parameters and subsequently adjusts and fits model parameters based on measurement data. This approach increases the model's complexity. Moreover, the GBSM, tailored to specific measurement environments, may exhibit biases in the fitting process, leading to inaccuracies in the model's characterization. Therefore, the GAN-GRU based joint predictive channel model can not only improve the efficiency and accuracy of the space-time joint channel prediction but also provide sufficient channel parameters to facilitate channel modeling.

Moreover, to provide a comprehensive assessment of the proposed GAN-GRU framework, additional experiments comparing its computational performance with alternative models are conducted on continuous datasets. As shown in Table V, the computational time required by each model was carefully measured and analyzed on the computer with INTEL i9 10980xe, RTX3090, and 64 GB RAM. The findings reveal that the GAN-GRU framework exhibits a notable advantage in processing efficiency compared to GAN-LSTM. Specifically, the coupled architecture of GAN-GRU demonstrates a shorter processing time while maintaining higher prediction accuracy. Except for optimizing for real-time processing time, it's essential to note that the primary focus of the proposed model is on offline data augmentation applications, emphasizing the accurate space-time joint channel prediction of unknown spatial positions and future time. While the usage of STGAN for data augmentation contributes to a certain increase in overall computational time compared with normal GRU and LSTM, it significantly increases the data augmentation ability and enhances the accuracy of the predictions. This trade-off ensures the reliability of the predictive results, which is crucial for successfully implementing the proposed space-time joint predictive channel model in practical scenarios.

2) Prediction Comparison on Discrete Channel Parameter Datasets: In this part, the proposed GAN-GRU framework is compared with RBF-NN, where RBF-NN is proven to

TABLE IV
THE PREDICTION PERFORMANCE COMPARISON ON THE CONTINUOUS SPACE-TIME CHANNEL DATASETS.

	2.4 GHz, LoS					**2.4 GHz, NLoS**				
	GAN-GRU	GAN-LSTM	GRU	LSTM	6GPCM	GAN-GRU	GAN-LSTM	GRU	LSTM	6GPCM
RMSE (dB)	**4.7908**	6.1363	9.7905	9.7442	10.4924	**5.5826**	6.0852	10.1082	10.8970	11.5807
MAPE (%)	**4.1363**	5.4093	6.9101	8.4023	8.9941	**5.0971**	5.9932	7.2895	8.8891	9.1440
	5 GHz, LoS					**5 GHz, NLoS**				
	GAN-GRU	GAN-LSTM	GRU	LSTM	6GPCM	GAN-GRU	GAN-LSTM	GRU	LSTM	6GPCM
RMSE (dB)	**5.3992**	6.9234	10.8716	11.3559	11.8428	**5.7475**	7.3466	11.2146	11.9702	12.8636
MAPE (%)	**4.8458**	5.4133	7.9936	8.4770	8.8114	**5.0339**	5.9522	8.0793	9.1003	9.7441
	6 GHz, LoS					**6 GHz, NLoS**				
	GAN-GRU	GAN-LSTM	GRU	LSTM	6GPCM	GAN-GRU	GAN-LSTM	GRU	LSTM	6GPCM
RMSE (dB)	**5.0375**	6.5363	10.7905	11.7442	11.8647	**5.6310**	7.1237	10.1164	11.2437	12.1878
MAPE (%)	**4.2090**	5.1093	7.9101	8.4023	8.7734	**4.6940**	5.3952	7.5823	8.0936	9.3266

TABLE V
THE COMPUTATIONAL TIME REQUIRED BY EACH MODEL.

	GAN-GRU	GAN-LSTM	GRU	LSTM
Time (min)	61	79	27	32

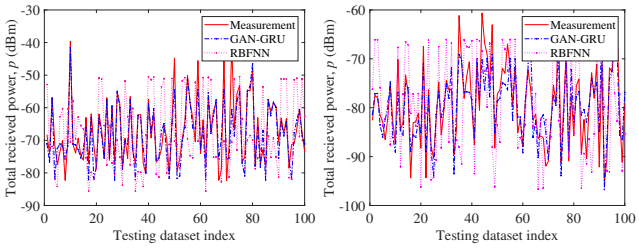

Fig. 12. The discrete channel parameter prediction results about received power: (a) LoS, and (b) NLoS.

TABLE VI
THE PREDICTION PERFORMANCE COMPARISON ON DISCRETE CHANNEL PARAMETER DATASETS.

	LoS		**NLoS**	
	GAN-GRU	RBF-NN	GAN-GRU	RBF-NN
RMSE (dB)	**2.0852**	5.2482	**2.4363**	6.2558
MAPE (%)	**1.9932**	4.8626	**2.1093**	5.5198

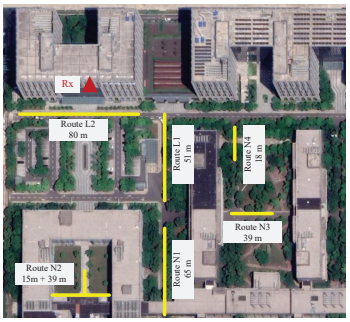

Fig. 13. The layout and antenna positions of the UMi scenario.

have better channel prediction performance than FNN in [19]. The discrete channel parameter dataset contains channel data with physical labels, where the channel data are discrete index parameters calculated from original continuous channel data and the data label refers to Rx positions. Based on the discrete dataset, the inputs of RBF-NN are the frequency bands and the Rx positions, and the prediction output is the total received power of the corresponding Rx position, which can be regarded as a single space domain predictive channel modeling separated from the space-time joint modeling. Firstly, the delay PSDs are obtained based on the original channel measurement data, and then the total received power at each Rx position is calculated by the integral of the delay PSDs. These discrete parameter datasets are divided into LoS and NLoS scenarios. LoS datasets contain 484 groups of the training set and 121 groups of the test set. NLoS datasets contain 516 groups of the training set and 129 groups of the test set.

The testing results, as shown in Fig. 12, demonstrate the performance of both the GAN-GRU framework and the RBF-NN. The abscissa represents the index of the testing dataset or the number of testing samples. From Table VI, it can be observed that both the GAN-GRU framework and the RBF-NN achieve good performance in predicting the discrete channel parameters and the GAN-GRU framework outperforms the RBF-NN in terms of prediction accuracy. Despite the slightly lower accuracy of the RBF-NN, its lower complexity enables faster training speed compared to the more sophisticated GAN-GRU framework. However, it is worth noting that the higher complexity of the GAN-GRU framework does not impact the efficiency and performance of the prediction process, as the space-time joint prediction is conducted offline.

From these two comparative experiments, it is proven that the accuracy achieved with the discrete channel parameter datasets is higher, indicating better fitting with the real channels. This is due to the simplicity of the structure in the discrete datasets, which does not require highly complex networks for training. As a result, the advantages of the proposed models may not be as apparent when predicting simple channel parameter data. However, the GAN-GRU framework demonstrates excellent performance in joint prediction using continuous space-time channel datasets, which are inherently

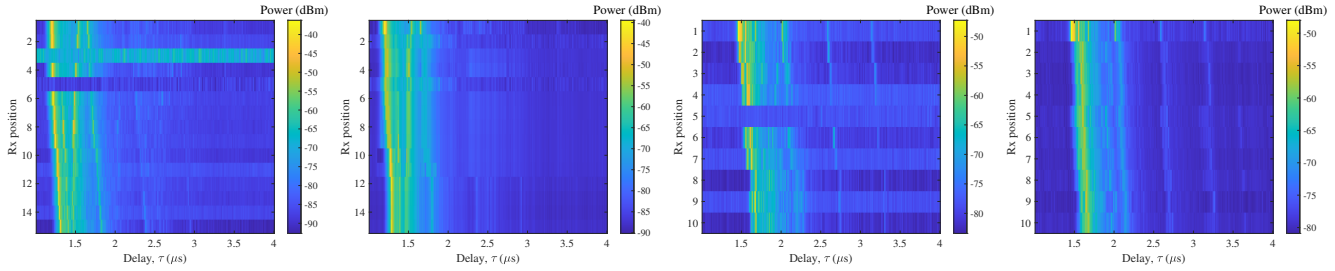

Fig. 14. The delay PSDs of measured channels and predicted channels at outdoor UMi scenario: (a) LoS measurement data, (b) LoS prediction data, (c) NLoS measurement data, and (d) NLoS prediction data.

more complex than discrete datasets. Consequently, compared to the RBF-NN, which is primarily suitable for discrete channel parameter prediction, the GAN-GRU framework exhibits better generalization and robustness.

E. Outdoor Channel Prediction Verification

To verify the proposed model is still valid for the outdoor channel prediction experiments, this section uses channel measurement data collected in an urban microcell (UMi) scenario as the validation dataset to show the generality of the proposed model. The buildings are located on the roads with an average height of 35 m, the roadside green belts and trees are distributed along the roads, and the interval between each building is approximately 30–40 m. Measurement campaigns include 4 cases including LoS and NLoS scenarios, as shown in Fig 13, and data of Route L1 and N1 are used as the reference to do the space-time joint channel prediction, where these routes are straight-line with typical space-time characteristics.

The results, as shown in Fig. 14, demonstrate the efficacy of the proposed model in accurately predicting the joint prediction of the paths with the strongest power, even in complex outdoor environments. The model successfully captures the drifting of paths along the delay axis, revealing the channel dynamic variations in the space-time domains. It effectively predicts the fluctuations and variations in the channel characteristics caused by factors such as multipath fading, shadowing, and scattering in outdoor scenarios. Notably, the proposed model exhibits remarkable adaptability in handling challenging scenarios, such as scenarios with significant path loss due to obstructions or NLoS conditions. Furthermore, the proposed model's ability to fix damaged channel data and compensate for abnormal data during channel measurements is also evident in these experiments. These observations confirm that the proposed model has a robust learning capacity, enabling it to handle unpredictable channel conditions and capture the intricate space-time variations in the outdoor MIMO channel. Overall, the results from this UMi scenario suggest that the proposed model is a promising solution for accurate space-time joint channel prediction in various environments.

VI. Conclusions

In this paper, a novel GAN-GRU based space-time joint predictive channel model has been proposed to effectively capture continuous channel variations at each location in a time series. The model's ability to predict channels in space-time domains and handle lost and abnormal data has highlighted its significance in space-time joint predictive channel modeling. We have shown that the STGAN framework in the proposed model can expand channel datasets and improve training performance by synthesizing channel datasets with the same space-time characteristics based on real channel measurement data. Moreover, we have demonstrated that the GRU framework can predict unknown channels in the space-time domains based on previous channels by continuous measurements after path identification. We have used channel measurement data conducted in the indoor corridor and outdoor UMi with typical space-time channel characteristics for performance validation to verify the proposed model. Comparative experiments with existing data augmentation methods have shown the good data augmentation performance of the proposed model. Then, optimal model settings have been obtained by analyzing the value of the channel memory parameter k. Through comprehensive experiments using indoor channel measurement datasets, we have demonstrated that the proposed model outperforms the 6GPCM and other ML-based methods, including GRU, LSTM, and RBF-NN, in terms of prediction performance. The model has been further verified using outdoor UMi channel measurement datasets, showing good performance. These experiments have illustrated the model's ability to synthesize channel data, rebuild lost data, correct abnormal data, and predict channels in the space-time domains. In summary, the proposed model has several advantages, including better prediction performance, robustness, and the ability to learn the space-time joint characteristics. This makes it a promising method for future research in channel prediction, which benefits wireless communication systems. In network planning and optimization, our model aids in optimizing coverage, distributing base stations, and achieving energy-efficient wireless communications. In wireless transmission, it facilitates improved system design, adjusted code modulation schemes, and efficient management of signal-to-noise ratios.

References

[1] C.-X. Wang, J. Huang, H. Wang, X. Gao, X.-H. You, and Y. Hao, "6G wireless channel measurements and models: Trends and challenges," *IEEE Veh. Technol. Mag.*, vol. 15, no. 4, pp. 22–32, Dec. 2020.

[2] H. Tataria, M. Shafi, A. F. Molisch, M. Dohler, H. Sjöland, and F. Tufvesson, "6G wireless systems: Vision, requirements, challenges, insights, and opportunities," *Proc. IEEE*, vol. 109, no. 7, pp. 1166–1199, July 2021.

[3] X.-H. You, C.-X. Wang, J. Huang, *et al.*, "Towards 6G wireless communication networks: Vision, enabling technologies, and new paradigm shifts," *Sci. China Inf. Sci.*, vol. 64, no. 1, Jan. 2021, doi: 10.1007/s11432-020-2955-6.

[4] C.-X. Wang, X. You, X. Gao, et al., "On the road to 6G: Visions, requirements, key technologies and testbeds," *IEEE Commun. Surveys Tuts.*, vol. 25, no. 2, pp. 905–974, 2nd Quart. 2023

[5] C.-X. Wang, J. Bian, J. Sun, W. Zhang, and M. Zhang, "A survey of 5G channel measurements and models," *IEEE Commun. Surveys Tuts.*, vol. 20, no. 4, pp. 3142–3168, 4th Quart. 2018.

[6] S. Bi, R. Zhang, Z. Ding, and S. Cui, "Wireless communications in the era of big data," *IEEE Commun. Mag.*, vol. 53, no. 10, pp. 190–199, Oct. 2015.

[7] X.-H. You, *et al.*, "AI for 5G: Research directions and paradigms," *Sci. China Inf. Sci.*, vol. 62, no. 2, pp. 1–13, Feb. 2019.

[8] M. Chen, U. Challita, W. Saad, C. Yin, and M. Debbah, "Artificial neural networks-based machine learning for wireless networks: A tutorial," *IEEE Commun. Surveys Tuts.*, vol. 21, no. 4, pp. 3039–3071, July 2019.

[9] C.-X. Wang, M. D. Renzo, S. Stanczak, S. Wang, and E. G. Larsson, "Artificial intelligence enabled wireless networking for 5G and beyond: Recent advances and future challenges," *IEEE Wireless Commun.*, vol. 27, no. 1, pp.16–23, Feb. 2020.

[10] Q. Wu, H. Wang, and W. Hong, "Multistage collaborative machine learning and its application to antenna modeling and optimization," *IEEE Trans. Antennas Propag.*, vol. 68, no. 5, pp. 3397–3409, Jan. 2020.

[11] R. He, B. Ai, G. Wang, M. Yang, and Z. Zhong, "Wireless channel sparsity: Measurement, analysis, and exploitation in estimation," *IEEE Wireless Commun.*, vol. 28, no. 4, pp. 113–119, Aug. 2021.

[12] Q. Hu, F. Gao, H. Zhang, S. Jin, and G. Y. Li, "Deep learning for channel estimation: Interpretation, performance, and comparison," *IEEE Trans. Wireless Commun.*, vol. 20, no. 4, pp. 2398–2412, Apr. 2021.

[13] C. Huang, *et al.*, "Artificial intelligence enabled radio propagation for communications–Part I: Channel characterization and antenna-channel optimization," *IEEE Trans. Antennas Propag.*, vol. 70, no. 6, pp. 3939–3954, June 2022.

[14] C. Huang, *et al.*, "Artificial intelligence enabled radio propagation for communications–Part II: Scenario identification and channel modeling," *IEEE Trans. Antennas Propag.*, vol. 70, no. 6, pp. 3955–3969, June 2022.

[15] U. Challita, L. Dong, and W. Saad, "Proactive resource management for LTE in unlicensed spectrum: A deep learning perspective," *IEEE Trans. Wireless Commun.*, vol. 17, no. 7, pp. 4674–4689, July 2018.

[16] M. Yang, *et al.*, "Machine learning-based fast angle-of-arrival recognition for vehicular communications," *IEEE Trans. Veh. Technol.*, vol. 70, no. 2, pp. 1592–1605, Feb. 2021.

[17] X. Zhao, *et al.*, "Playback of 5G and beyond measured MIMO channels by an ANN-based modeling and simulation framework," *IEEE J. Sel. Areas Commun.*, vol. 38, no. 9, pp. 1945–1954, Sept. 2020.

[18] B. Hua, *et al.*, "Channel modeling for UAV-to-Ground communications with posture variation and fuselage scattering effect," *IEEE Trans. Wireless Commu.*, vol. 71, no. 5, pp. 3103–3116, May 2023.

[19] J. Huang, C.-X. Wang, L. Bai, *et al.*, "A big data enabled channel model for 5G wireless communication systems," *IEEE Trans. Big Data*, vol. 6, no. 2, pp. 211–222, June 2020.

[20] L. Bai, Q. Xu, S. Wu, S. Ventouras, and G. Goussetis, "A novel atmosphere-informed data-driven predictive channel modeling for B5G/6G satellite-terrestrial wireless communication systems at Q-Band," *IEEE Trans. Veh. Technol.*, vol. 69, no. 12, pp. 14225–14237, Dec. 2020.

[21] S. R. Mattu, L. N. Theagarajan, and A. Chockalingam, "Deep channel prediction: A DNN framework for receiver design in time-varying fading channels," *IEEE Trans. Veh. Technol.*, vol. 71, no. 6, pp. 6439–6453, June 2022.

[22] Y. Yang, F. Gao, Z. Zhong, B. Ai, and A. Alkhateeb, "Deep transfer learning-based downlink channel prediction for FDD massive MIMO systems," *IEEE Trans. Commun.*, vol. 68, no. 12, pp. 7485–7497, Dec. 2020.

[23] L. Liu, L. Cai, L. Ma, and G. Qiao, "Channel state information prediction for adaptive underwater acoustic downlink OFDMA system: Deep neural networks based approach," *IEEE Trans. Veh. Technol.*, vol. 70, no. 9, pp. 9063-9076, Sept. 2021.

[24] L. Yu and C.-X. Wang, "Prediction of wireless mmWave massive MIMO channel characteristics based on graph attention networks," in *Proc. ICETC'20*, Tokyo, Japan, Dec. 2020, pp. 1-5.

[25] Z. Li, C.-X. Wang, C. Huang, L. Yu, J. Li, and Z. Qian, "A novel scatterer density-based predictive channel model for 6G communications," in *Proc. IEEE VTC'23-Spring*, Florence, Italy, June 2023, pp. 1–5.

[26] I. Goodfellow, *et al.*, "Generative adversarial nets," *Adv. NIPS*, vol. 27, Jan. 2014.

[27] Y. Yang, Y. Li, W. Zhang, F. Qin, P. Zhu, and C.-X. Wang, "Generative-adversarial-network-based wireless channel modeling: Challenges and opportunities," *IEEE Commun. Mag.*, vol. 57, no. 3, pp. 22–27, Mar. 2019.

[28] S. Seyedsalehi, V. Pourahmadi, H. Sheikhzadeh, and A. H. G. Foumani, "Propagation channel modeling by deep learning techniques," *arXiv:1908.06767*, Aug. 2019.

[29] H. Xiao, W. Tian, W. Liu and J. Shen, "ChannelGAN: Deep learning-based channel modeling and generating," *IEEE Wireless Commun. Lett*, vol. 11, no. 3, pp. 650–654, Mar. 2022.

[30] Z. Liu, Z. Teng, Y. Song, X. Ye, and Y. Ouyang, "Channel modeling and generation: Train generative networks and generate 6G channel data," in *Proc. IEEE ICCC'22*, Chengdu, China, Dec. 2022, pp. 72–78.

[31] Y. Zhang, *et al.*, "Generative adversarial networks based digital twin channel modeling for intelligent communication networks," *China Commun.*, vol. 20, no. 8, pp. 32–43, Aug. 2023.

[32] K. Mao, *et al.*, "Machine-learning-based 3-D channel modeling for U2V mmWave communications," *IEEE Internet Things J.*, vol. 9, no. 18, pp. 17592–17607, Sept. 2022.

[33] C.-X. Wang, Z. Lv, X. Gao, X.-H. You, Y. Hao, and H. Haas, "Pervasive wireless channel modeling theory and applications to 6G GBSMs for all frequency bands and all scenarios," *IEEE Trans. Veh. Technol.*, vol. 71, no. 9, pp. 9159–9173, Sept. 2022.

[34] Z. Li, C.-X. Wang, J. Huang, W. Zhou, and C. Huang, "A GAN-LSTM based AI framework for 6G wireless channel prediction," in *Proc. IEEE VTC'22-Spring*, Helsinki, Finland, June 2022, pp. 1-5.

[35] J. W. McKown and R. L. Hamilton, "Ray tracing as a design tool for radio networks," *IEEE Netw.*, vol. 5, no. 6, pp. 27–30, Nov. 1991.

[36] D. He, B. Ai, K. Guan, L. Wang, Z. Zhong, and T. Kürner, "The design and applications of high-performance ray-tracing simulation platform for 5G and beyond wireless communications: A tutorial," *IEEE Commun. Surveys Tuts.*, vol. 21, no. 1, pp. 10–27, Aug. 2019.

[37] F. H. Tanaka, D. S. Kiyoiti, and A. Claus, "Data augmentation using GANs," *arXiv: 1904.09135*, Apr. 2019.

[38] M. Mehdi and S. Osindero, "Conditional generative adversarial nets," *arXiv: 1411.1784*, Nov. 2014.

[39] R. Casas, A. Macro, J. J. Guerrero, and J. Falco, "Robust estimator for non-line-of-sight error mitigation in indoor localization," *EURASIP J. Adv. Signal Process.*, pp. 1–8, Dec. 2006.

[40] G. Van Houdt, C. Mosquera, and G. Nápoles, "A review on the long short-term memory model," *Artif. Intell. Rev.*, vol. 53, no. 8, pp. 5929–5955, Dec. 2020.

[41] J. Chung, C. Gulcehre, K. Cho, and Y. Bengio, "Empirical evaluation of gated recurrent neural networks on sequence modeling," *arXiv:1412.3555*, Dec. 2014.

[42] H. Xu, V. Kukshya, and T. S. Rappaport, "Spatial and temporal characteristics of 60-GHz indoor channels," *IEEE J. Sel. Areas Commun.*, vol. 20, no. 3, pp. 620–630, Apr. 2002.

[43] Z. Zhou, L. Zhang, X. Chen, C.-X. Wang, and J. Huang, "Multi-frequency wireless channel measurements and characteristics analysis in indoor corridor scenarios," in *Proc. IEEE VTC'21-Fall*, Norman, OK, USA, Sept. 2021, pp. 1–5.

[44] V. Kristem, S. Sangodoyin, C. Bas, et al., "3D MIMO outdoor-to-indoor propagation channel measurement," *IEEE Trans. Wireless Commun.*, vol. 16, no. 7, pp. 4600–4613, July 2017.

[45] J. Huang, C. -X. Wang, H. Chang, J. Sun, and X. Gao, "Multi-frequency multi-scenario millimeter wave MIMO channel measurements and modeling for B5G wireless communication systems," *IEEE J. Sel. Areas Commun.,* , vol. 38, no. 9, pp. 2010–2025, Sept. 2020.

[46] 3GPP, Tech. Rep. 38.901, "Study on channel model for frequencies from 0.5 to 100 GHz (Release 16),". [Online]. Available: https://portal.3gpp.org/desktopmodules/Specifications/SpecificationDetails.aspx?specificationId=3173, Nov. 2020.

[47] D. P. Kingma and J. Ba, "Adam: A method for stochastic optimization," *arXiv: 1412.6980*, Dec. 2014.

[48] A. Radford, L. Metz, and S. Chintala, "Unsupervised representation learning with deep convolutional generative adversarial networks," *arXiv: 1511.06434*, Jan. 2015.

[49] M. Arjovsky, S. Chintala, and L. Bottou1, "Wasserstein GAN," *arXiv: 1701.07875*, Dec. 2017.